Available online at www.sciencedirect.com
SCIENCE DIRECT®
Composites Science and Technology 66 (2006) 1195–1201
COMPOSITES SCIENCE AND TECHNOLOGY
www.elsevier.com/locate/compscitech

Surface-initiated polymerization from TiO_2 nanoparticle surfaces through a biomimetic initiator: A new route toward polymer–matrix nanocomposites

Xiaowu Fan, Lijun Lin, Phillip B. Messersmith *

Department of Biomedical Engineering, Robert R. McCormick School of Engineering and Applied Sciences, Northwestern University, 2145 Sheridan Road, E374 TECH Bldg., Evanston, IL 60208, United States

Received 5 October 2005; accepted 5 October 2005
Available online 15 November 2005

Abstract

Polymer nanocomposites of core–shell structure were prepared by grafting poly(methyl methacrylate) (PMMA) from TiO_2 nanoparticle via the surface-initiated polymerization (SIP) strategy. A bifunctional polymerization initiator inspired by L-3,4-dihydroxyphenylalanine (DOPA), a key constituent of mussel adhesive proteins (MAPs), was designed and synthesized for use in SIP from oxide surfaces. The biomimetic initiator spontaneously adsorbed to TiO_2 from aqueous solution, resulting in a colloidal initiator system with the initiator content of approximately 6.8 wt%. Subsequent in situ activation of the surface-initiated atom transfer radical polymerization (SI-ATRP) gave rise to PMMA polymer shell layers tethered to TiO_2 nanoparticle cores. The results demonstrate a viable biomimetic strategy toward the preparation of polymer functionalized metal oxide nanoparticles that may be useful for construction of functional polymer nanocomposites.

Keywords: A. Polymer–matrix composites; D. Infrared spectroscopy; D. Thermogravimetric analysis; E. Surface-initiated polymerization

1. Introduction

Polymer–matrix nanocomposites (PMNs) represent an attractive family of composite materials in which the nanometer-size reinforcing fillers are uniformly dispersed in the polymer matrix on a nanometer scale as compared to conventional phase-separated macrocomposites [1]. Due to the high surface areas of the nanofillers and their molecular-level interactions with the polymer chains, there is great interest in nanocomposites due to significant scientific questions relating to interfacial chemistry and physics as well as their greatly enhanced practical properties [2]. Polymer-clay nanocomposites (PCNs), which are probably the most intensively investigated PMN system to date, serve as typical examples that exhibit highly improved thermal, mechanical, and barrier properties achieved at substantially low filler contents (usually <5 wt%) because of the total exfoliation and nanometer-scale dispersion of layered silicate platelets in the polymer matrix [3,4].

In addition to physical methods that essentially involve blending polymers with original or organically modified fillers, surface-initiated polymerization (SIP) is a promising and versatile approach among various chemical synthesis methods for the preparation of PMNs [5]. In SIP, a polymerization initiator is first anchored to the nano-filler surface by chemi- or physisorption and then activated in situ in the presence of monomers under polymerization conditions. Thus, SIP generates a PMN in which the polymer chains are bound to the nanofiller surface. The basic advantage of SIP originates from a sound assumption that exfoliation could be facilitated by polymer chains growing from nanofiller surfaces, leading to finely dispersed PMNs. Moreover, SIP is capable of producing polymer-coated

* Corresponding author. Tel.: +1 847 467 5273; fax: +1 847 491 4928.
E-mail address: philm@northwestern.edu (P.B. Messersmith).

0266-3538/$ - see front matter © 2005 Elsevier Ltd. All rights reserved.
doi:10.1016/j.compscitech.2005.10.001

precursor nanofillers that provide better dispersiblity and compatibility with the polymer matrix in the physical methods for PMNs [6].

Because of their interesting mechanical, electronic, optical, catalytic, and magnetic characteristics, SIP has also been developed into a powerful strategy for modifying and tailoring the surface properties of metal and semiconductor nanospheres, oxide nanospheres and nanorods, and carbon nanotubes toward nanostructured functional materials [7]. Since Prucker and Ruhe first demonstrated the SIP approach with silica nanoparticles in 1998 [8], it has been utilized to graft different polymers from a wide range of surfaces, such as flat oxide substrates [9], spherical nanoparticles [10,11], planar clay nanoplatelets [12–14], and cylindrical carbon nanotubes [15,16], etc. Polymerization mechanisms proven successful by SIP include traditional free radical polymerization [17,18], nitroxide-mediated stable free radical polymerization (SFRP) [19], living anionic polymerization [20,21], and atom transfer radical polymerization (ATRP) [22]. Surface-initiated ATRP (SI-ATRP) has been used to graft polymers from various metal oxides including alumina [23], iron oxide [24], and titanium oxo clusters systems [25].

In this paper, we report our initial results on the preparation of poly(methyl methacrylate) (PMMA)-modified TiO_2 nanofiller using a biomimetic initiator capable of strong adsorption to TiO_2 surfaces. We are especially interested in using SIP strategy from TiO_2 surface because the grafted polymer chains are believed to increase the affinity of the inorganic oxide filler to organic solvents and polymer matrices [26,27]. In order to apply the SIP approach to Ti/TiO_x surfaces, we designed and synthesized a biomimetic initiator inspired by adhesive proteins that are secreted by mussels to adhere to various marine and freshwater surfaces. These mussel adhesive proteins (MAPs) were found to have a high concentration of a catecholic amino acid, L-3,4-dihydroxyphenylalanine (DOPA) [28–30], which is believed to interact strongly with a variety of metal, metal oxide, and polymers [31,32]. Hence, the biomimetic bifunctional initiator contains a catechol end to anchor to TiO_2 surface and a bromine terminus to activate ATRP (Scheme 1). The biomimetic concept has been demonstrated by our previous work on incorporating DOPA in biocompatible polymers for bioadhesive hydrogels [33,34] and in non-fouling polymer–peptide conjugates to modify Ti/TiO_x substrates [35]. In this study, we intend to graft PMMA shell layers from ~34 nm diameter TiO_2 nanoparticle core via SI-ATRP. High surface area TiO_2 nanoparticle was used as a model system to study the feasibility of this biomimetic approach to SI-ATRP from oxide nanoparticles.

2. Experimental

2.1. Materials

Titanium dioxide nanoparticles (Nano Tek® Titanium dioxide, average particle size 34 nm, BET specific surface area 45 m^2/g, 80% anatase and 20% rutile) was purchased from Nanophase Technologies Corporation (Romeoville, IL). Ultrapure water (resistivity = 18.2 MΩ, pH 6.82) used in all experiments was obtained from a NANOpure Infinity® system from Barnstead/Thermolyne Corporation (Dubuque, IA). MMA monomer (99%, Aldrich) was distilled at reduced pressure before polymerization. Catechol (99%, Sigma), Copper (I) bromide (CuBr, 99.999%, Aldrich), *N*,*N*,*N*′,*N*′,*N*″-Pentamethyldiethylenetriamine (PMDETA, 99%, Aldrich), Aliquat 336 (Aldrich), and hydrofluoric acid (~49 wt% HF in water, Fisher) were used as received. Other reagents and organic solvents for the initiator synthesis and polymerization were purchased from commercial sources and used without further purification.

2.2. Initiator immobilization

The synthesis and characterization of the SI-ATRP initiator (Scheme 1) has been recently reported [36]. 250 mg TiO_2 powder was dispersed in 250 mL ultrapure water, followed by ultrasonication for 30 min and overnight stirring, to yield a white homogeneous dispersion. 21.6 mg (0.075 mmol) initiator was dissolved in 10 mL ultrapure water with the aid of ultrasonication. The white TiO_2 dispersion turned yellow upon dropwise addition of the initiator solution while stirring at room temperature. After stirring the mixture in the dark for 24 h, the yellow precipitates were obtained by gravity filtration through a hydrophilic nylon membrane filter. The precipitates were then re-dispersed in 250 mL ultrapure water and filtered again. This washing process was repeated three times to eliminate unbound initiator. About 225 mg of TiO_2–initiator complex was collected and stored in an amber glass vial after drying under vacuum for 24 h. In order to study the interaction between the catechol part of the initiator and TiO_2 nanoparticle, a reference sample consisting of TiO_2 and pure catechol was also prepared using the same procedures.

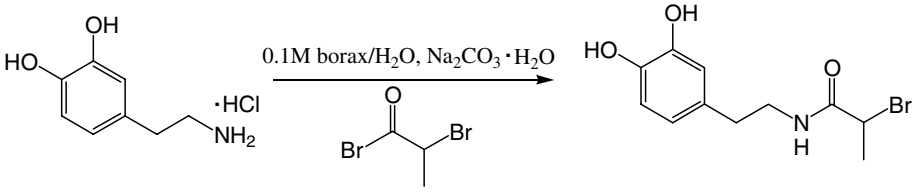

Scheme 1. Synthetic scheme and structure of the catechol-terminated SI-ATRP initiator.

2.3. SI-ATRP procedure

In a typical polymerization, 100 mg TiO_2–initiator complex was dispersed in 50 mL *N*,*N*-dimethylformamide (DMF). The mixture was ultrasonicated until a homogeneous yellow mixture was observed. After purging for 1 hour under Ar flow, 4.3 mg (0.03 mmol) CuBr and 6.25 μL (0.03 mmol) PMDETA were added. The system was purged with Ar for 1 hour. 10 mL (93.6 mmol) MMA was injected via a degassed syringe, the temperature increased to 65 °C and the reaction held under Ar protection for up to 28 h. Samples were extracted via a degassed syringe at defined intervals during the polymerization. The samples were centrifuged at 8000 rpm for 10 min, followed by decantation of the supernatant liquid. The pellet was redispersed in DMF and centrifuged again. This washing process was repeated with THF and acetone to remove the catalyst, monomer, and free polymer that were not bound to the TiO_2 nanoparticle surfaces. The remaining solids were dried under vacuum for 24 h. To isolate the polymer bound to the TiO_2 surface, the polymer-grafted TiO_2 sample was dispersed in 1 mL toluene along with 2 mg Aliquat 336 (phase transfer catalyst) and 1 mL 49 wt% HF aqueous solution. The mixture was allowed to stir for 24 h, during which time the TiO_2 dissolved. Polymer was recovered by precipitation into cold methanol and filtration.

2.4. Characterization and instrumentation

Fourier transform infrared (FT-IR) spectra of original and modified TiO_2 samples were obtained on a Thermo Nicolet NEXUS 870 system. Dried solids were pressed with KBr (FT-IR grade, Aldrich) and the pellets were scanned 64 times using transmission mode with a resolution of 4 cm^{-1}. UV–Vis spectra were recorded on a Varian Cary 1E model spectrophotometer. Pure and modified TiO_2 powders were measured by using the diffuse reflectance module. Thermogravimetric analysis (TGA) traces were obtained on a SDT 2960 model from TA Instruments. All measurements were performed under nitrogen flow with a heating rate of 20 °C/min. The powder samples were dried under vacuum overnight to remove moisture before analysis. Transmission electron microscopy (TEM) images were acquired on a Hitachi H-8100 electron microscope operated at 200 kV. TEM specimens were prepared by casting drops of dilute dispersion of polymer-grafted TiO_2 nanoparticles in acetone on 200-mesh carbon-supported copper grids.

Gel permeation chromatography (GPC) traces were obtained on a Waters 515 HPLC system with UV–Vis and refractive index detectors and THF as the eluent. PMMA standards (Pressure Chemicals, Pittsburgh, PA) were used to determine the molecular weight (MW) and polydispersity index (PDI) of the PMMA sample. Samples were filtered using 0.2 μm Teflon syringe filters before injection to remove insoluble residue.

3. Results and discussion

3.1. Preparation and characterization of the colloidal initiator

It is well known that catechol derivatives can form stable complexes with the surface metal atoms of certain metal oxides [37]. Surface complexation with catechol compounds was used to modify the surface electronic state of colloidal semiconductors such as TiO_2 nanoparticle [38]. In our case, the strong interaction between catechol and TiO_2 was utilized to immobilize the bifunctional initiator for SI-ATRP from TiO_2 nanoparticle surfaces (Scheme 2).

FT-IR spectra of pure TiO_2, pure initiator, and TiO_2–initiator complex are shown in Fig. 1. Besides the strong peak at 1651 cm^{-1} that comes from amide C=O stretching of the pure initiator molecule, other absorption bands that are associated with the catechol moiety can be assigned as previously shown [39]. Strong bands at 1522 and 1566 cm^{-1} are assigned to aromatic C–C stretching. Multiple peaks from 1250 to 1450 cm^{-1} can be attributed to phenolic O–H deformations coupled/decoupled with C–C ring stretching and phenolic C–O stretching. Multiple bands between 1200 and 1000 cm^{-1} result from phenolic C–O stretching and aromatic C–H in-plane bending.

In the spectrum of the TiO_2–initiator complex, peaks due to C–O stretching and C–H bending were still present but shifted to a broad peak at 1211 cm^{-1} with a shoulder at 1238 cm^{-1} and another peak at 1157 cm^{-1}. The former band can be attributed to C–O vibrations after chemisorption that was present at about 1250 cm^{-1} in the spectrum

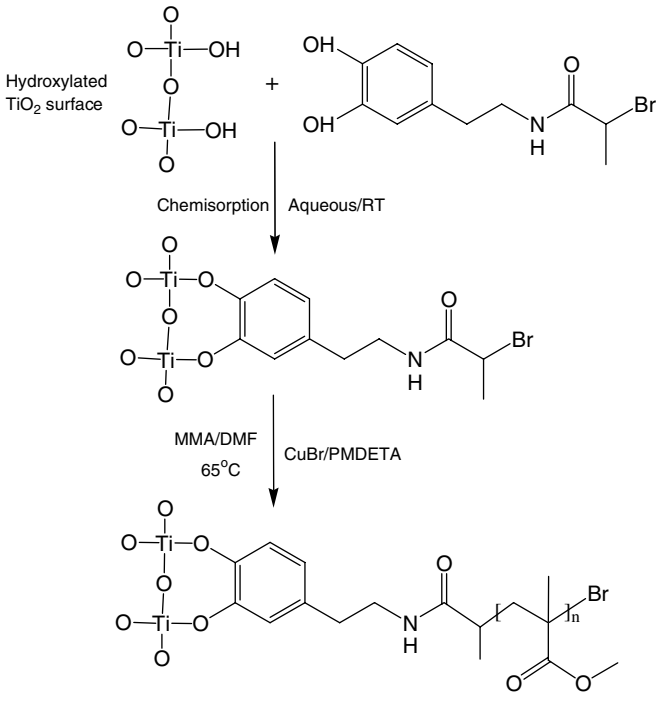

Scheme 2. Initiator immobilization and SI-ATRP (only the binuclear chelation is shown).

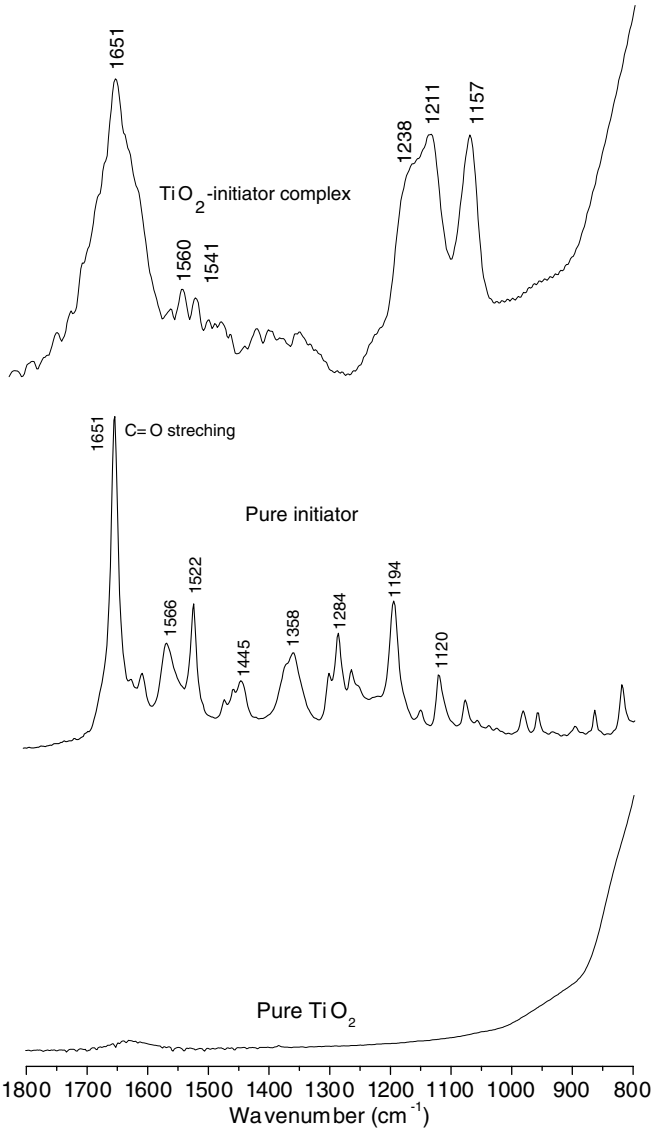

Fig. 1. FTIR spectra of pure initiator and initiator modified TiO_2.

of TiO_2–pure catechol complex (not shown) as well as in those of other studies on the complexation between catechol derivatives and TiO_2 [40,41]. The increase of the spectrum baseline below 1100 cm^{-1} is due to strong absorbance from Ti–O/O–O bonds in TiO_2 lattice which is also shown in the lower wavenumber region in the spectrum of pure TiO_2 sample. Furthermore, the strong peak at 1651 cm^{-1} from carbonyl group stretching still remained after surface complexation, which clearly confirmed the presence of the initiator on the TiO_2 nanoparticle. Previous FT-IR investigations suggested that the chemisorption of catechol onto the TiO_2 surface involved the deprotonation of the phenolic hydroxyl groups of the catechol and its subsequent bidentate chelation to the surface Ti [41,42]. A similar mechanism is suggested by the FT-IR spectrum of the TiO_2–initiator complex. First, absorbance of the peaks at 1522 and 1566 cm^{-1} from C–C ring stretching was reduced after the initiator's attachment to the TiO_2 surface. This is probably due to the decrease of the mobility of the C–C ring vibrations that are close to the surface binding site. Secondly, multiple peaks from 1250 to 1450 cm^{-1} from phenolic O–H vibrations practically disappeared owing to the deprotonation of the phenolic OH groups in the surface chelation process.

UV–Vis diffuse reflectance measurements also demonstrate the presence of the catechol moiety of the initiator on the TiO_2 surface. Fig. 2 shows the UV–Vis absorption of pure TiO_2, TiO_2 colloidal initiator, and TiO_2–catechol complex. Pure TiO_2 nanoparticle shows the typical absorption edge at 400 nm [37,38]. In comparison, TiO_2–catechol complex displays a broad shoulder that reaches a maximum absorbance at about 420 nm. The spectrum of TiO_2–initiator complex also shows a broad band at 420 nm and closely resembles the overall features of that of the TiO_2–pure catechol complex. This broad band can be attributed to the intramolecular ligand-to-metal charge transfer transition within the surface Ti–catechol complex, in which light with a wavelength of around 420 nm can activate electron transfer from the surface complexant to the conduction band of TiO_2 [38]. Similar UV–Vis features were observed for the interactions between various metal oxides including TiO_2 and catechol derivatives [43–45]. Thus, both IR and UV–Vis results clearly demonstrate that the catechol-terminated initiator molecule is indeed immobilized to the nanoparticle surface through the interaction between catechol moiety and TiO_2.

TGA was used to quantitatively obtain the content of initiator in the TiO_2–initiator complex. Fig. 3 shows the thermal decomposition behaviors of pure TiO_2, TiO_2–initiator complex, and pure initiator. The weight loss of pure TiO_2 was about 2.3% when heated from room temperature to 800 °C, which was mostly due to the evaporation of absorbed water. The pure initiator did not show any significant decomposition below approx. 200 °C, which suggests the unbound initiator possesses the necessary thermal stability for the subsequent SI-ATRP. Above 200 °C, the ini-

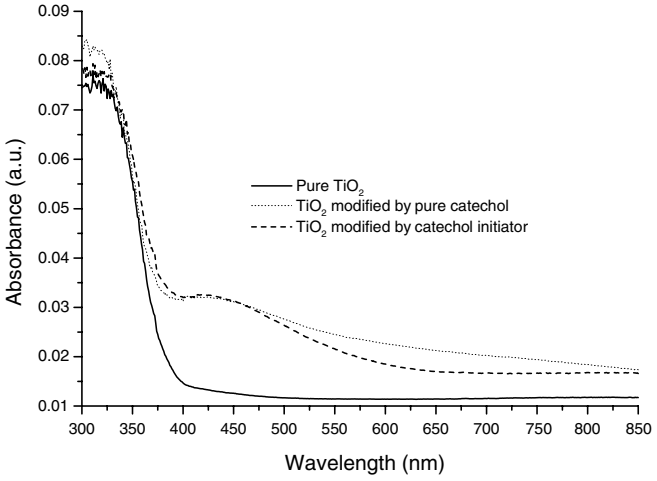

Fig. 2. UV–Vis diffuse reflectance spectra of pure TiO_2, TiO_2 modified with initiator, and TiO_2 modified with catechol.

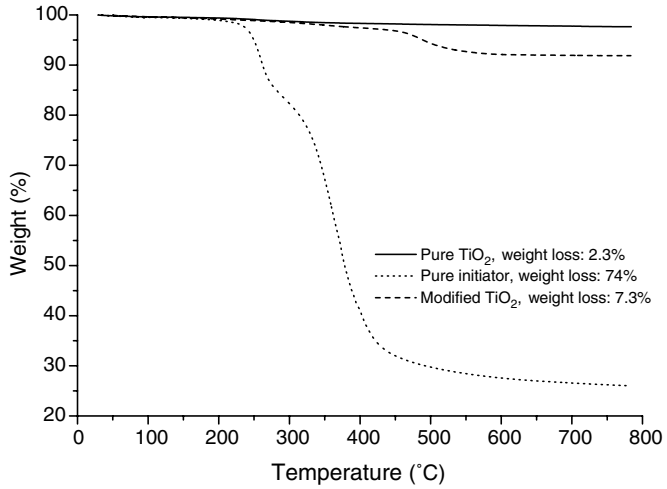

Fig. 3. TGA traces of TiO_2 nanoparticle, TiO_2–initiator complex, and pure initiator.

tiator showed two significant thermal degradations, from 200 to 300 °C and from 300 to 500 °C. The first degradation was consistent with the degradation of the catechol moiety, which occurred at a similar temperature range for the pure catechol (thermogram not shown), whereas the second thermal degradation was likely due to the decomposition of the alkyl spacer and the amide group.

The thermal degradation behavior of the TiO_2–initiator complex was qualitatively similar to that of the pure initiator, although the degradation of the adsorbed initiator occurred at higher temperatures. Given that the strong affinity between catechol and TiO_2 originates from the reaction between OH groups that are linked to surface Ti atoms and the phenolic OH groups in catechol [45], the content of the initiator in the modified TiO_2 was expected to be related to the specific surface area and surface density of the Ti sites on the nanoparticle surface. The specific surface area of the TiO_2 nanoparticle had an average value of 45 m^2/g. Based on another commercial TiO_2 material (Degussa P-25) with similar average surface area (50 m^2/g) and composition (20% rutile and 80% anatase), the surface density of OH groups should range from 1.7 to 3.3 hydroxyl/nm^2 [45,46]. The excessive amount of initiator we used was calculated from an arbitrary value of 4 hydroxyl/nm^2. Based on this value, the theoretical initiator content was calculated to be 8% for mononuclear chelation and 4% for binuclear chelation. Experimentally, the TGA weight loss for the modified TiO_2 was approx. 7.3%. Assuming that the pristine and modified TiO_2 had the same level of moisture, the initiator content from TGA weight loss could be estimated as: (7.3–2.3%)/(1–26%) = 6.8%. This value is between and in agreement with the theoretical values considering the two chelation possibilities.

3.2. SI-ATRP

The bifunctional initiator was designed to provide robust anchoring to the TiO_2 surface via the catechol moiety, whereas the alkyl halide permitted ATRP from the functionalized TiO_2 surface. DMF, which has relatively high polarity, was chosen as the polymerization solvent because the structural similarity among DMF solvent, MMA monomer, and the initiator afforded a homogeneous and efficient polymerization system. Previous studies demonstrated that homogeneity of the polymerization dispersion that contained inorganic colloidal initiator, organic solvent and monomer was crucial for monomer diffusion toward surface and successful growth of polymer brushes [17,21].

Successful SI-ATRP of MMA was demonstrated by FT-IR, TGA, and TEM analysis of TiO_2 nanoparticles after polymerization followed by washing with excess solvents and drying under vacuum. Fig. 4 illustrates an IR spectrum of a PMMA-grafted TiO_2 sample after 24 h of polymerization at 65 °C. The expected C–H vibrations at 2950 cm^{-1} and carbonyl stretching at 1730 cm^{-1} clearly indicate the presence of PMMA in the sample. In addition, the amide band at 1650 cm^{-1} indicates the presence of the initiator moiety (Scheme 1) and that the grafted PMMA was indeed formed through our proposed SI-ATRP scheme. The amounts of grafted PMMA at different polymerization times were determined by TGA. As shown in Fig. 5, thermograms of PMMA-grafted TiO_2 exhibit a major decomposition event at about 400 °C, which is due to the decomposition of grafted PMMA polymer. As shown in Fig. 6, the mass growth of grafted PMMA (determined by TGA weight loss) on the TiO_2 nanoparticle was nearly linear. Moreover, the successful grafting of PMMA was also confirmed by TEM observation. Fig. 7 is a representative image that shows an individual grafted nanoparticle consisting of a dark core of TiO_2 surrounded by a light polymer shell. It can be seen that, after 20 h of SI-ATRP, the particle diameter grew to ~60 nm from its ~35 nm TiO_2 core, which is consistent with the average size of the pristine nanoparticles.

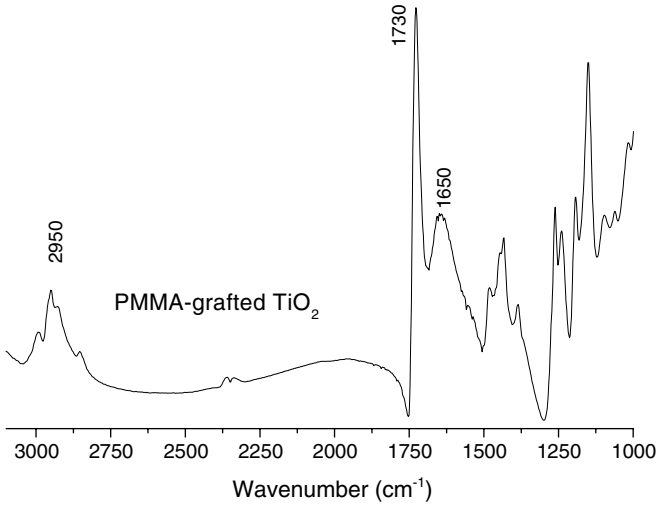

Fig. 4. FT-IR spectrum of PMMA-grafted TiO_2 nanoparticle after 24 h polymerization.

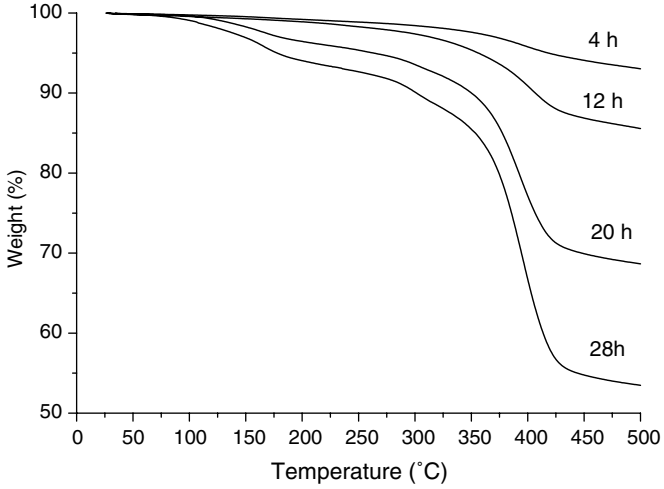

Fig. 5. TGA thermograms of PMMA-grafted TiO_2 nanoparticle at different polymerization times.

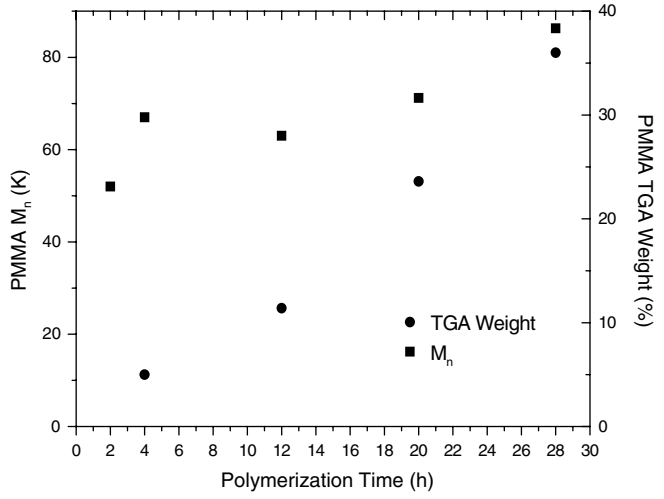

Fig. 6. Bound PMMA mass and $\bar{M}_n$ as a function of polymerization time.

Our results indicate that the bifunctional initiator adsorbed to TiO_2 nanoparticle surfaces and was capable initiating ATRP of MMA from the nanoparticle surface. Dissolution of the TiO_2 nanoparticle in HF, followed by MW analysis of the bound polymer, revealed that the PMMA MW reached a relatively high MW ($\bar{M}_n \sim 52$ K) within 2 h. As shown in Fig. 6, further increase in polymerization time resulted in a modest increase in MW with a maximum of $\bar{M}_n \sim 83$ K. Meanwhile, the polydispersities of bound PMMAs were determined to be in the range of 1.5–1.9.

The lack of precise kinetic and MW control of bound PMMA suggests that the ATRP conditions were not ideal in this case. Previous studies have shown that ATRP of MMA is relatively hard to control for both neat and SIPs [47–49]. It has been demonstrated that copper-mediated ATRP of MMA has a significantly higher equilibrium constant compared with other monomers such as styrene and methyl acrylate, which makes the ATRP of MMA rather facile but relatively difficult to control [47]. Similar to our

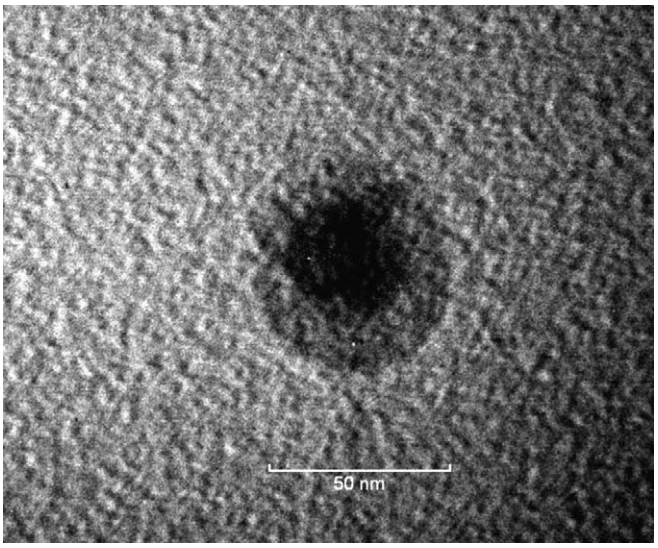

Fig. 7. TEM micrograph of PMMA-grafted TiO_2 nanoparticle after 20 h of SI-ATRP.

results of rapid chain growth and high polydispersity, poor MW control of grafted PMMA was also observed for modified silica nanoparticles [48] and single-walled carbon nanotubes as ATRP macroinitiators [49]. Generally, MW control in ATRP is achieved by the persistent radical effect, in which the termination of less than 5% of the short chains leads to the initial concentration increase of the deactivator (Cu^{II} compound) to protect the growing radicals during later stages of the polymerization [50]. In the case of SI-ATRP, sufficient deactivator concentration is unlikely to attain due to the very low concentration of the immobilized initiator. Therefore, a low deactivator concentration results in fast and uncontrolled chain growth and termination. In our SI-ATRP, we used a high monomer to initiator ratio (~3000) to achieve high MW polymer grafted from TiO_2 nanoparticle surfaces, which has been supported by the above TGA and GPC results. However, the controllability of graft polymerization was sacrificed by the extremely low initiator concentration.

Another possibility for poor control of ATRP may originate from the phenolic groups on the catechol end of the bifunctional initiator, which may be expected to impede the polymerization through the abstraction of the phenolic hydrogen to inhibit the radical chain growth. However, Haddleton et al. studied the copper-mediated ATRP of MMA in the presence different phenolic compounds, and found them to accelerate the rate of ATRP instead [51]. Thus, any residual, unbound free initiators that were not completely washed away in the preparation of the TiO_2–initiator complex could influence the SI-ATRP process as well as initiate ATRP in the free medium. This may explain why some free PMMA was also observed in the centrifuge supernatants. Measured by GPC, the MWs and PDIs of free PMMAs showed similar values to those of bound PMMAs (data not shown). Previous studies have shown better-controlled MW growth can be achieved by adding either "free/

sacrificial initiator" or radical deativator (Cu^{II} species) at the beginning of the SI-ATRP from flat substrates [52,53], silica nanoparticles [48], and carbon nanotubes [54]. Efforts to improve the controllability of our biologically inspired SI-ATRP strategy are currently underway.

4. Conclusions

A biomimetic initiator inspired by MAPs and DOPA was synthesized for SI-ATRP. The initiator was successfully anchored to TiO_2 nanoparticle surfaces by aqueous chemisorption, which was confirmed by FT-IR and UV–Vis spectroscopy. TGA showed an initiator content of 6.8 wt%, which was in agreement with the surface hydroxyl group density. Initial FT-IR, TGA, and TEM results from SI-ATRP of MMA proved the feasibility of the biomimetic polymer grafting strategy, although further work toward better MW control of the grafted PMMA is desired through optimization of ATRP conditions. Above all, this viable approach can be applied to other metal oxide fillers and substrates with polymers of diverse functionalities, and may open a new route to the modification of nanofillers and the preparation of functional PMNs and ultrathin films.

Acknowledgments

This project is supported by the Biologically Inspired Materials (BIMat) program under the University Research, Engineering, and Technology Institute (URETI) of NASA (Grant No. NCC-1-02037). Dr. Nianqiang Wu and Dr. Shuyou Li at Northwestern University NU*ANCE* center are acknowledged for their assistance on FT-IR and TEM analysis.

References

[1] Pinnavaia TJ, Beall GW. Polymer-clay nanocomposites. Wiley series in polymer science. Chichester: Wiley; 2000.
[2] Giannelis EP, Krishnamoorti R, Manias E. Adv Polym Sci 1999;138:108–47.
[3] Kojima Y, Usuki A, Kawasumi M, Okada A, Fukushima Y, Kurauchi T, et al. J Mater Res 1993;8(5):1185–9.
[4] Alexandre M, Dubois P. Mater Sci Eng R 2000;28(1–2):1–63.
[5] Fan X, Xia C, Advincula RC. Polymer-clay nanocomposites and polymer brushes from clay surfaces. In: Schwarz JA, Contescu CI, Putyera K, editors. Dekker encyclopedia of nanoscience and nanotechnology, vol. 4. New York: Marcel Dekker; 2004. p. 2959–71.
[6] Pyun J, Matyjaszewski K. Chem Mater 2001;13(10):3436–48.
[7] Advincula RC. J Dispersion Sci Tech 2003;24(3–4):343–61.
[8] Prucker O, Ruhe J. Macromolecules 1998;31(3):592–601.
[9] Zhao B, Brittain WJ. Prog Polym Sci 2000;25(5):677–710.
[10] Perruchot C, Khan MA, Kamistsi A, Armes SP, von Werne T, Patten TE. Langmuir 2000;17(15):4479–81.
[11] Ohno K, Koh K-m, Tsujii Y, Fukuda T. Macromolecules 2002;35(24):8989–93.
[12] Zhao H, Shipp D. Chem Mater 2003;15(14):2693–5.
[13] Fan X, Xia C, Fulghum T, Park M-K, Locklin J, Advincula RC. Langmuir 2003;19(3):916–23.
[14] Bottcher H, Hellensleben ML, Nub S, Wurm H, Bauer J, Behrens P. J Mater Chem 2002;12:1351–4.
[15] Kong H, Gao C, Yan D. J Am Chem Soc 2004;126(2):412–3.
[16] Qin S, Qin D, Ford WT, Resasco DE, Herrera JE. J Am Chem Soc 2004;126(1):170–6.
[17] Fan X, Xia C, Advincula RC. Langmuir 2003;19(10):4381–9.
[18] Huang X, Brittain WJ. Macromolecules 2001;34(10):3255–60.
[19] Weimer MW, Chen H, Giannelis EP, Sogah DY. J Am Chem Soc 1999;121(7):1615–6.
[20] Zhou Q, Wang S, Fan X, Advincula RC, Mays J. Langmuir 2002;18(8):3324–31.
[21] Fan X, Zhou Q, Xia C, Christofoli W, Mays J, Advincula RC. Langmuir 2002;18(11):4511–8.
[22] Pyun J, Kowalewski T, Matyjaszewski K. Macromol Rapid Commun 2003;24(18):1043–59.
[23] Gu B, Sen A. Macromolecules 2002;35(23):8913–6.
[24] Vestal CR, Zhang ZJ. J Am Chem Soc 2002;124(48):14312–3.
[25] Kickelbick G, Holzinger D, Brick C, Tremmel G, Moons E. Chem Mater 2002;14(10):4382–9.
[26] Shirai Y, Kawatsura K, Tsubokawa N. Prog Org Coat 1999;36(4):217–24.
[27] Shirai Y, Tsubokawa N. React Funct Polym 1997;32(2):153–60.
[28] Waite JH, Tanzer ML. Science 1981;212:1038–40.
[29] Yamamoto H. Biotechnol Genet Eng Rev 1996;13:133–65.
[30] Sever M, Weisser JT, Monahan J, Srinivasan S, Wilker JJ. Angew Chem Int Ed 2004;43(4):448–50.
[31] Ooka AA, Garrell LR. Biopolymers 2000;57(2):92–102.
[32] Yu M, Hwang J, Deming TJ. J Am Chem Soc 1999;121(24):5825–6.
[33] Huang K, Lee BP, Ingram D, Messersmith PB. Biomacromolecules 2002;3(2):397–406.
[34] Lee BP, Dalsin JL, Messersmith PB. Biomacromolecules 2002;3(5):1038–47.
[35] Dalsin JL, Hu B-H, Lee BP, Messersmith PB. J Am Chem Soc 2003;125(14):4253–8.
[36] Fan X, Lin L, Dalsin JL, Messersmith PB. J Am Chem Soc 2005, in preparation.
[37] Rajh T, Chen LX, Lukas K, Liu T, Thurnauer MC, Tiede DM. J Phys Chem B 2002;106(41):10543–52.
[38] Moser J, Punchihewa S, Infelta PP, Gratzel M. Langmuir 1991;7(12):3012–8.
[39] McBride MB, Wesselink LG. Environ Sci Technol 1988;22(6):703–8.
[40] McWhirter MJ, Bremer PJ, Lamont IL, McQuillan AJ. Langmuir 2003;19(9):3575–7.
[41] Martin ST, Kesselman JM, Park DS, Lewis NS, Hoffmann MR. Environ Sci Technol 1996;30(8):2535–42.
[42] Connor PA, Dobson KD, McQuillan AJ. Langmuir 1995;11(11):4193–5.
[43] Borgias BA, Cooper SR, Koh YB, Raymond KN. Inorg Chem 1984;23(8):1009–16.
[44] Tachikawa T, Tojo S, Fujitsuka M, Majima T. Langmuir 2004;20(7):2753–9.
[45] Rodriguez R, Blesa MA, Regazzoni AEJ. Colloid Interface Sci 1996;177(1):122–31.
[46] Erdem B, Hunsicker RA, Simmons GW, Sudol ED, Dimonie VL, El-Aasser MS. Langmuir 2001;17(9):2664–9.
[47] Queffelec J, Gaynor SG, Matyjaszewski K. Macromolecules 2000;33(23):8629–39.
[48] von Werne T, Patton TE. J Am Chem Soc 2001;123(31):7497–505.
[49] Yao Z, Braidy N, Botton GA, Adronov A. J Am Chem Soc 2003;125(51):16015–24.
[50] Matyjaszewski K, Pattern TE, Xia J. J Am Chem Soc 1997;119(4):674–80.
[51] Haddleton DM, Clark AJ, Crossman MC, Duncalf DJ, Heming AM, Morsley SR, et al. Chem Commun 1997;13:1173–4.
[52] Ejaz M, Yamamoto S, Ohno K, Tsujii Y, Fukuda T. Macromolecules 1998;31(17):5934–6.
[53] Kim J-B, Huang W, Miller MD, Baker GL, Bruening ML. J Polym Sci Polym Chem 2003;41(3):386–94.
[54] Qin S, Qin D, Ford WT, Resasco DE, Herrera JE. Macromolecules 2004;37(3):752–3.